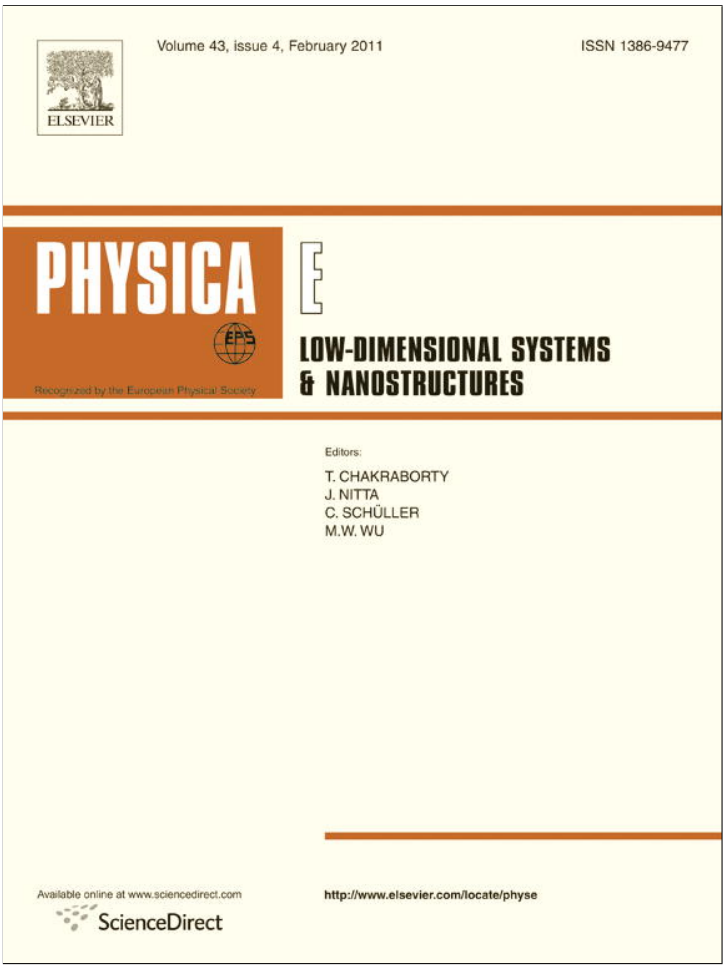

Physica E 43 (2011) 857–861

Contents lists available at ScienceDirect

Physica E

journal homepage: www.elsevier.com/locate/physe

Fabrication and characterization of TiO_2–ZnO composite nanofibers

A.F. Lotus [a], S.N. Tacastacas [b], M.J. Pinti [b], L.A. Britton [c], N. Stojilovic [d,*], R.D. Ramsier [c,e,f], G.G. Chase [a]

[a] Department of Chemical and Biomolecular Engineering, The University of Akron, Akron, OH 44325, USA
[b] Physics Department, John Carroll University, University Heights, OH 44118, USA
[c] Department of Chemistry, The University of Akron, Akron, OH 44325, USA
[d] Department of Physics and Astronomy, University of Wisconsin Oshkosh, Oshkosh, WI 54901, USA
[e] Department of Physics, The University of Akron, Akron, OH 44325, USA
[f] Office of the Provost, The University of Akron, Akron, OH 44325, USA

ARTICLE INFO

Article history:
Received 2 November 2009
Received in revised form
11 September 2010
Accepted 27 October 2010
Available online 31 October 2010

ABSTRACT

Tetraisopropyl titanate, zinc acetate dihydrate, and polyvinylpyrrolidone (PVP) were mixed to obtain a composite solution for producing TiO_2–ZnO nanofibers. Electrospinning and subsequent calcination at 973 K were employed to produce composite metal-oxide nanofibers with diameters ranging from 50 to 150 nm. Characterization of the TiO_2–ZnO composite nanofibers was carried out by thermogravimetric analysis (TGA), scanning electron microscopy (SEM), X-ray energy dispersive spectroscopy (XEDS), X-ray diffraction (XRD), X-ray photoelectron spectroscopy (XPS), Fourier transform infrared spectroscopy (FTIR), and ultraviolet–visible (UV–vis) spectrophotometry. TGA reveals a total weight loss of 49% and no change in mass above 873 K. The nanofibers are predominantly made of titania and exhibit two different energy band gap values of 3.0 and 3.5 eV. Our findings indicate that in the composite TiO_2–ZnO nanofibers three different phases (anatase and rutile TiO_2 and wurtzite ZnO) can co-exist and retain their individual characteristic properties.

1. Introduction

Electrospinning is a relatively simple and inexpensive top-down method for producing non-woven nanofibers [1–9]. The chemical composition as well as physical and chemical properties of the electrospun nanofibers can be tailored by selecting suitable polymers and other organic and/or inorganic components. Most of the literature on electrospinning focuses on polymeric nanofibers, whereas the application of this process to the fabrication of metal-oxide nanofibers is relatively new. The preparation of metal-oxide nanofiber composites is challenging but can potentially lead to novel structures with the combined attributes of the constituent materials. This can be achieved by varying precursor ratios and tailoring the crystal structures during calcination. These mixed metal-oxide ceramic nanofiber structures can be flexible and withstand high temperatures and are, therefore, attractive materials for use in a variety of applications.

TiO_2 has a wide band gap—$E_g \cong 3.0$ eV for the rutile phase and $E_g \cong 3.2$ eV for the anatase phase, and is a promising material for use in photocatalysis [10,11] and thermophotovoltaics [12]. On the other hand, ZnO, also a wide band gap material ($E_g \cong 3.4$ eV), is of current interest for blue/UV optoelectronic applications and potential spintronic devices [13,14]. Both titania (TiO_2) [12,15–21] and zinc oxide (ZnO) [22–25] electrospun nanofibers have been fabricated and characterized previously. Also, electrospun ceramic $BaTiO_3$ [26] and ZnO–NiO composite nanofibers [27,28] have also been reported. The surface area of nanofibrous structures can be several orders of magnitude higher than that of thin films, which results in higher sensitivity and faster responses in sensor applications [29], where we believe composite metal-oxide nanofibers could find applications.

The main goal of this study is to demonstrate that electrospinning, as an easily accessible method, can be successfully employed to fabricate composite TiO_2–ZnO nanofibers. The resulting fibers are characterized using a range of analytical methods, which include thermogravimetric analysis (TGA), scanning electron microscopy (SEM), X-ray energy dispersive spectroscopy (XEDS), X-ray diffraction (XRD), X-ray photoelectron spectroscopy (XPS), Fourier transform infrared spectroscopy (FTIR), and ultraviolet–visible (UV–vis) spectrophotometry.

2. Experimental procedures

2.1. Fabrication

The electrospinning solution was prepared in multiple steps, in which individual precursor solutions for zinc oxide and titania

* Corresponding author. Tel.: +1 920 424 4431.
E-mail address: stojilovicn@uwosh.edu (N. Stojilovic).

1386-9477/$ - see front matter © 2010 Elsevier B.V. All rights reserved.
doi:10.1016/j.physe.2010.10.015

were prepared and then mixed together with a polymeric solution to obtain a viscous, transparent, homogeneous composite solution.

Step 1: To make the precursor solution for ZnO, zinc acetate dihydrate ($Zn(CH_3COO)_2 \cdot 2H_2O$) was used as the starting material, and 2-methoxyethanol and monoethanolamine (MEA) were used as a solvent and stabilizer, respectively. Zinc acetate dihydrate was first dissolved in a mixture of 2-methoxyethanol and MEA solution at room temperature. The MEA to zinc acetate ($Zn(CH_3COO)_2$) molar ratio in the solution was 1.0 and was mixed in the 2-methoxyethanol solvent to yield a concentration of zinc acetate of 0.35 M. This mixture was stirred at 333 K for 2 h until it became clear and homogeneous, which served as the precursor solution for ZnO on cooling to room temperature.

Step 2: Tetraisopropyl titanate, an organic alkoxy titanate was used as the precursor for titania as obtained from Du Pont (TYZOR® TPT, TiO_2 content 28.1%). It is a clear, colorless to yellowish liquid, which is very sensitive to moisture.

Step 3: To achieve the proper viscosity for electrospinning a solution was prepared by mixing 1.0 g of polyvinylpyrrolidone (PVP, Aldrich, molecular weight 1 300 000) with 17 ml of absolute ethanol (Pharmco). The mixture was stirred continuously while keeping the temperature constant at 313 K for 2 h and a viscous, clear solution was obtained.

Step 4: The solutions of TYZOR TPT, $Zn(Ac)_2$, and PVP were all mixed together at a volume ratio of 7:3:10 with constant stirring at 313 K to obtain a homogeneous, transparent, yellow colored, composite solution.

Step 5: This solution was electrospun at a constant flow rate of 6 μl/min using a syringe pump. The applied voltage was kept constant at 20 kV, and the pipette–collector gap distance was maintained at 20 cm. Electrospinning was carried out at room temperature and atmospheric pressure, with aluminum foil as the substrate for collecting nanofibers.

Step 6: The as-spun fibers were calcined at 973 K from ambient conditions at a heating rate of 10 K/min and were held at that temperature for 2 h to obtain ceramic TiO_2–ZnO fibers. Cooling was done in ambient condition (without any forced air circulation).

2.2. Characterization

The electrospun fibers were analyzed using a range of analytical techniques. TGA was performed using a Thermal Analyst 5000 with a Hi-Res TGA 2950 Thermogravimetric Analyzer, an air flow rate of 60 cm^3/min, and a heating rate of 10 K/min. SEM images were acquired using Hitachi S-2150 at an accelerating voltage of 50 kV. The bulk elemental composition of the fibers was analyzed using XEDS (FEI Quanta 200) operating at 25 kV. A VG ESCALAB MK II system with a hemispherical analyzer, and an Al anode X-ray source, operating at either 160 or 180 W, was used for the XPS measurements at a pressure below 1×10^{-8} mbar.

In addition, a Phillips PW3710 X-Ray Powder Diffractor (XRD) with copper Kα X-rays ($\lambda = 0.154$ nm) was employed for diffraction analysis with an accelerating voltage of 45 kV and a current of 40 mA. FTIR measurements were conducted on an evacuated Bruker IFS 66v/s spectrometer using a diffuse reflectance (DRIFTS) accessory at pressures below 5 mbar. UV–vis spectrophotometry was accomplished using a Cary 300 visible–UV spectrophotometer made by Varian in diffuse reflectance mode.

3. Results and discussion

Fig. 1 displays the change in the weight of the as-spun fibers versus temperature, starting from room temperature up to 1273 K. A total weight loss of 49% takes place in three steps. First, there is a 20% loss between room temperature and 548 K, followed by 19% between 548 and 613 K, and finally 10% between 613 and 873 K. Following the evaporation of water and trapped solvent, along with the removal of polymer, there is no change in weight above 873 K and, therefore, no change in the elemental composition of the composite TiO_2–ZnO nanofibers. This suggests that the desired calcination temperature lies above 873 K. On the other hand, heating nanofibers above 873 K is expected to result in enhanced anatase-to-rutile phase conversion. In this study we make an attempt to produce a mixture of three phases, anatase and rutile titania along with the wurtzite ZnO structure. For this purpose we calcined the composite nanofibers at 973 K.

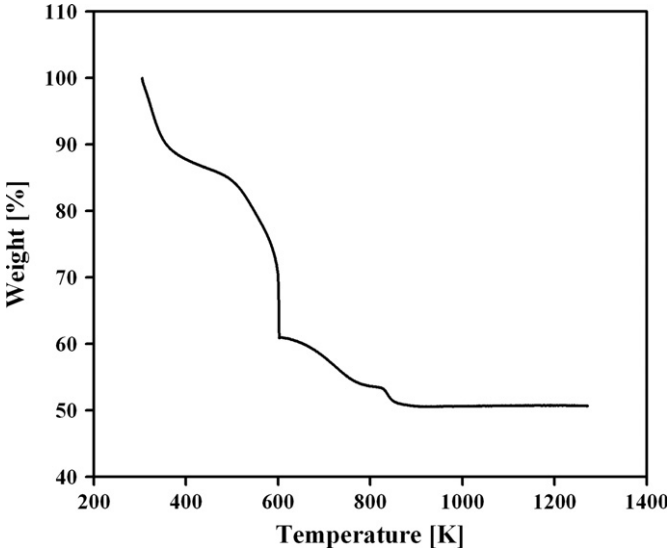

Fig. 1. Thermogravimetric analysis of as-spun fibers.

The representative morphology of the TiO_2–ZnO nanofibers is displayed in Fig. 2. The inset represents a high-resolution image of the non-woven mat. In this study we focused on the calcined nanofibers as they are of primary interest for potential applications, and we did not monitor changes in morphology of the fibers as a function of temperature. The average diameter of the calcined nanofibers was in the 50–150 nm range, and the high-resolution image (inset) reveals the dispersion of nanocrystals along the fiber surfaces, with the average particle size of about 10 nm. No such dispersion of nanoparticles has previously been reported for TiO_2 [12,15–21] and ZnO [22–25] nor for the composite ZnO–NiO [27,28] nanofibers. It is reasonable to conclude that the dispersion of nanoparticles occurs during the calcination process consistent with our XRD results (no indication of any crystal structure of pre-calcined samples). To further support our assumption that the dispersed particles are ZnO crystallites we will later estimate their size from XRD experiments using the Scherrer formula and compare the value with the size estimated from SEM measurements (see the inset of Fig. 2).

It is of interest to probe the elemental composition of the composite nanofibers, and for that purpose we used XEDS and XPS methods. Fig. 3 shows XEDS data from the calcined TiO_2–ZnO composite nanofibers. The very small Zn signature reveals that the fibers are predominantly composed of titania. The elemental composition of the calcined nanofibers, obtained from XEDS analysis and expressed in terms of atomic percentages, is as follows: 19% Ti, 1% Zn, and 80% O. These percentages were calculated using O–K, Zn–K, and Ti–K signals. Part of the oxygen signal originates from the sample mounting assembly whereas the carbon signal is not included in the analysis. XEDS measurements of the as-spun fibers (not shown) showed a much greater carbon signal, as expected. However, within the experimental uncertainty

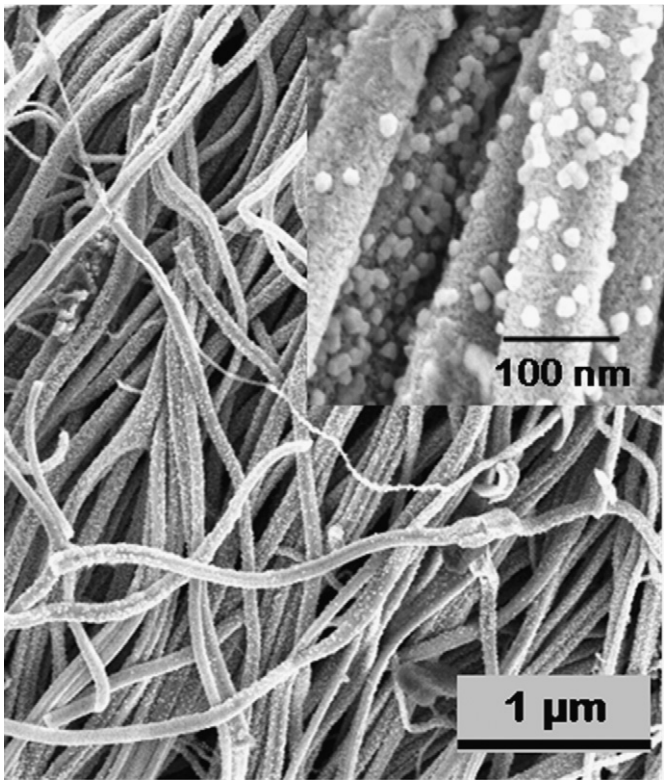

Fig. 2. Scanning electron micrograph of calcined TiO_2–ZnO nanofibers with the high-resolution image shown in the inset.

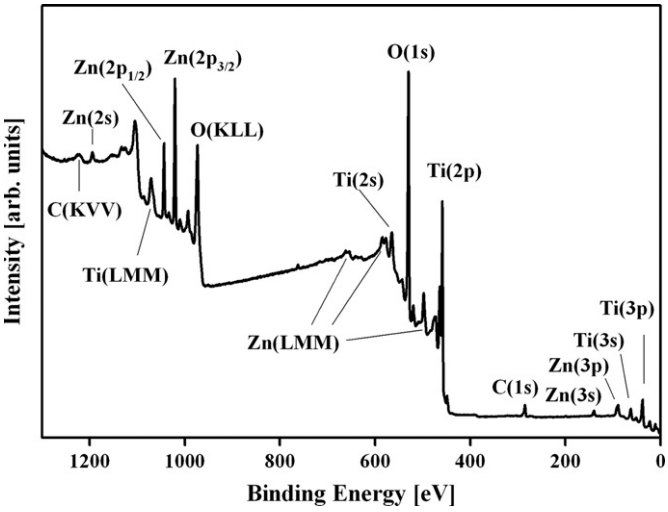

Fig. 3. X-ray energy dispersive spectroscopy results of calcined TiO_2–ZnO nanofibers.

of our XEDS measurements we find no significant difference between the Zn-to-Ti atomic ratios of the fibers versus that of the electrospinning solution. XEDS is sensitive to the bulk of the fibers as well as the surface containing the dispersed nanoparticles as the high-energy electrons used in these experiments have large penetration depth and the emitted X-rays have a long mean free path. We conclude, therefore, that the nanoparticles dispersed along the surface of the nanofibers during calcination are not likely to dominate the XEDS measurements.

The XPS data of Fig. 4 clearly show the presence of Ti, Zn, and O and traces of carbon. Since sputtering of the nanofibers was not performed to avoid damaging them, the carbon signal due to surface contamination is expected, as observed in related studies [21,30,31]. The calculated atomic percentages (disregarding carbon) based on our XPS results are as follows: 26% Ti, 6% Zn, and 68% O. These values were calculated using O(1s), Ti(2p), and Zn(2p) signatures. The XPS results show that the surface of the nanofibers is primarily composed of titania similar to the XEDS results. However, surface-sensitive XPS measurements show larger quantities of Zn than that indicated by the bulk-sensitive XEDS experiments and these two methods complement each other. The combined XEDS and XPS results suggest that the nanoparticles residing on the surface of the fibers are most likely ZnO.

Fig. 5 shows XRD data from the calcined nanofibers. A mixture of the three phases is evident. Anatase (A) and rutile (R) phases of titania, together with the wurtzite ZnO, are present. The rutile phase is the thermodynamically more stable form of titania, and is the dominant phase in these fibrous structures. Wurzite features have been reported for ZnO nanofibers [22–25], and in ZnO–NiO nanofiber composites [27,28]. It is useful to obtain the approximate crystallite size from the Scherrer formula, $S = C_S\lambda/W\cos\theta$, where S is the size of crystallite, C_S is the Scherrer constant, which takes values between 0.9 and 1.2 depending on the shape of the particles, W is the full width at half maximum (FWHM) of the diffraction peak, and λ is the wavelength of the incident X-rays (0.154 nm). S is equal to or smaller than the grain size. We estimate the average linear dispersion of ZnO crystallites to be 6 nm, which is slightly smaller than the value obtained from high-resolution SEM measurements. Also, we do not have any clear evidence of mutual solubility of the oxides in the temperature range studied and our results suggest that the ZnO particles form in a dispersed manner on the predominantly titania nanofibers.

In our laboratories, TiO_2 nanofibers have previously been studied and changes in the titania crystal phases as a function of temperature have been observed, with a range of temperatures in which these two TiO_2 phases co-exist. In the case of pure titania electrospun nanofibers calcined at 973 K [21], we did not observe dispersion of nanocrystals along the surface of nanofibers. These facts, together with results from XPS and XEDS, support our hypothesis that the dispersed nanoparticles in our SEM images are most likely ZnO nanoparticles in the form of nanocrystals. However, we cannot completely rule out that some ZnO is present within the fibers or that some other stoichiometric forms of the oxides exist.

Fig. 6 displays an FTIR spectrum of the calcined TiO_2–ZnO composite nanofibers. The broad feature below 1000 cm^{-1} is the result of overlapping Ti–O and Zn–O modes. The two features observed between 1200 and 1600 cm^{-1} are most likely $HTiO^-$ and/or HTiOH signatures, respectively [32]. These FTIR results are very similar to those reported for TiO_2 nanofibers [21], which is to be expected since our composite metal-oxide nanofibers contain larger quantities of TiO_2. The main difference between the FTIR spectra of our current (TiO_2–ZnO) and previous results (TiO_2) [21] is that the Ti–O feature at 800 cm^{-1} is much broader due to overlapping with Zn–O in the TiO_2–ZnO fibers. We also observed O–H and CO_2 signatures, consistent with our previous study [21].

Fig. 7 displays UV–vis diffuse reflectance data from TiO_2–ZnO nanofibers calcined at 973 K. Since our composite metal-oxide nanofibers are primarily composed of three different crystal phases (anatase and rutile titania, and wurtzite zinc oxide) and since both titania and zinc oxide are wide band gap oxides it is reasonable to expect the composite TiO_2–ZnO nanofibers to have similar band gap energy values. To measure band gap energy values we employed the Kubelka–Munk method, as used in a related study on alumina–titania nanofibers [33]. In particular, the UV–vis data are presented as modified Kubelka–Munk function $[F(r)E]^{1/2}$ versus photon energy, E, where r is the reflectance and $F(r)$ is the Kubelka–Munk function. This plot is used to estimate the band gap

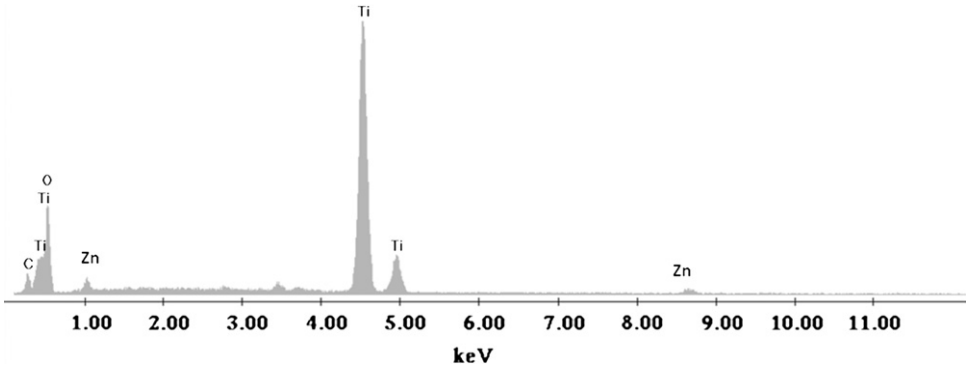

Fig. 4. X-ray photoelectron spectrum of calcined TiO_2–Zn nanofibers.

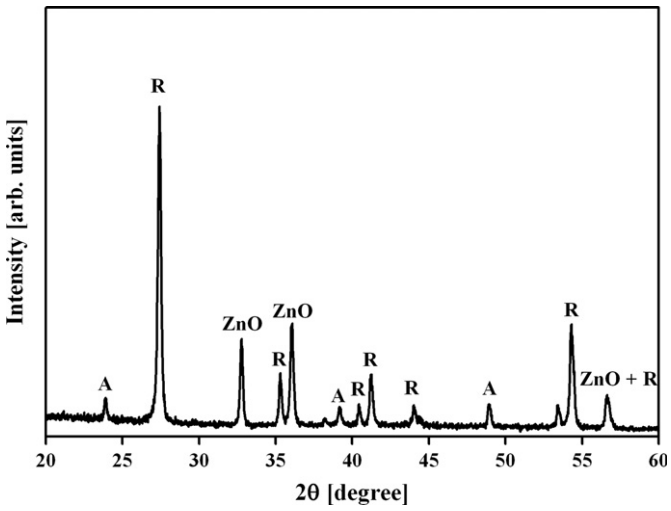

Fig. 5. X-ray diffraction pattern of calcined TiO_2–ZnO nanofibers.

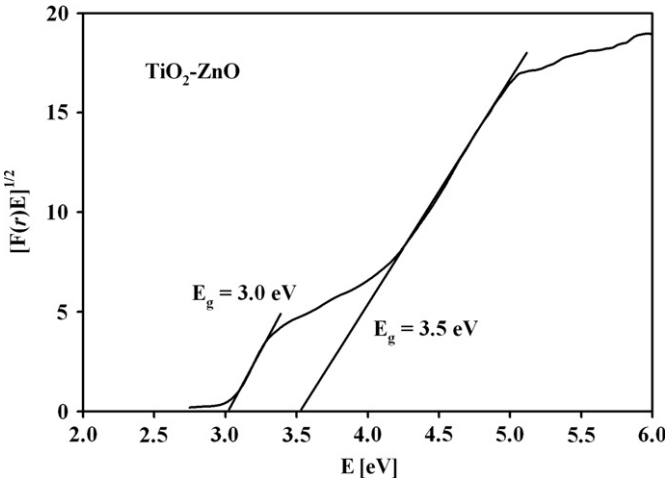

Fig. 7. UV–vis diffuse reflectance spectrum represented as modified Kubelka–Munk function versus photon energy.

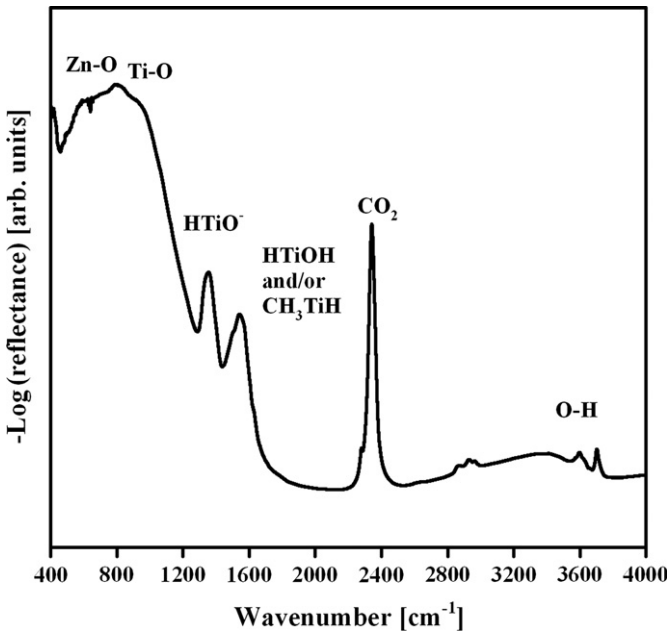

Fig. 6. Mid-infrared spectrum of calcined TiO_2–ZnO nanofibers.

energy (the point of the intercept of the tangent line with the energy axis) of the nanofibers. We find two values, E_g=3.0 and 3.5 eV. The lower value is close to that of rutile titania ($E_g \approx 3.0$ eV) whereas the greater value is closer to that of ZnO ($E_g \approx 3.4$ eV) and the anatase phase ($E_g \approx 3.2$ eV) of titania. Two different band gap energy values have previously been reported in a study on carbon-doped TiO_2 [34]. The fact that optical band gaps of rutile TiO_2 and ZnO seem to be preserved (within the experimental uncertainty of our measurements) in the composite nanofibers is consistent with our XRD data, where we see no phases such as $ZnTiO_3$. On the other hand, in a recent study on electrospun ZnO nanofibers it has been reported that Al-doping can affect the optical properties of the fibers [35]. The optical properties of the electrospun metal-oxide nanofibers in general can be tailored by mixing or doping with suitable species and selecting adequate calcination temperatures. We point out that in the case of composite nanofibers the optical band gap energy values can either be preserved or changed depending on whether phases separate or not. In the present case, the separation of phases maintains the individual crystal structures and band gaps of the components. We also wish to emphasize that relatively simple UV–vis diffuse reflectance measurements are a powerful tool in probing the energy band gaps of calcined fibers. These findings are, therefore, not only interesting from the standpoint of sensing applications but are also relevant for the photocatalytic applications.

4. Summary

TiO_2–ZnO composite nanofibers have been successfully produced using an electrospinning method and subsequent calcination at 973 K. TGA showed a total weight loss of 49% and no change in weight above 900 K. SEM measurements revealed diameters of the resulting fibers ranging from 50 to 150 nm and dispersion of nanoparticles along the surface of the nanofibers. The estimated linear dimension of the nanoparticles is around 10 nm. Elemental composition analysis of the composite nanofibers was conducted using XEDS and XPS, revealing that ZnO crystals favor the surface region of the nanofibers. The following three crystal phases are observed in the XRD measurements: anatase (A) and rutile (R) TiO_2, together with the wurtzite ZnO structure. FTIR analysis showed a broad feature below 1000 cm^{-1} due to overlap of the TiO_2 and ZnO phases. We used the Kubelka–Munk method for band gap energy calculations and found values of 3.0 and 3.5 eV. Since electrospinning is a relatively simple and inexpensive method for successful manufacturing of these nanofibers, we believe that these metal-oxide nanostructures could be utilized in numerous applications.

Acknowledgements

This work was supported by NSF, grants IIP 0637539 and DMI-0403835. We thank S.V. Dordevic for access into his UV–vis system, R.H. Seiple for TGA measurements, and E. Bender for acquisition of the XPS spectra. Finally, we thank an anonymous referee for critical reading and comments that helped us improve our manuscript.

References

[1] D.H. Reneker, I. Chun, Nanotechnology 7 (1996) 216.
[2] T. Subbiah, G.S. Bhat, R.W. Tock, S. Parameswaran, S.S. Ramkumar, J. Appl. Polym. Sci. 96 (2005) 557.
[3] C. Burger, B.S. Hsiao, B. Chu, Annu. Rev. Mater. Res. 36 (2006) 333.
[4] Z.-M. Huang, Y.-Z. Zhang, M. Kotaki, S. Ramakrishna, Compos. Sci. Technol. 63 (2003) 2223.
[5] K. Jayaraman, M. Kotaki, Y. Zhang, X. Mo, S. Ramakrishna, J. Nanosci. Nanotechnol. 4 (2004) 52.
[6] D. Li, Y. Xia, Adv. Mater. 16 (2004) 1151.
[7] A. Frenot, I.S. Chronakis, Curr. Opin. Colloid Interface Sci. 8 (2003) 64.
[8] J.B. Chiu, Y.K. Luu, D. Fang, B.S. Hsiao, B. Chu, M. Hadjiargyrou, J. Biomed. Nanotechnol. 1 (2005) 115.
[9] I.S. Chronakis, J. Mater. Process. Technol. 167 (2005) 283.
[10] A. Wold, Chem. Mater. 5 (1993) 280.
[11] M.R. Hoffmann, S.T. Martin, W. Choi, D.W. Bahnemann, Chem. Rev. 95 (1995) 69.
[12] V. Tomer, R. Teye-Mensah, J.C. Tokash, N. Stojilovic, W. Kataphinan, E.A. Evans, G.G. Chase, R.D. Ramsier, D.J. Smith, D.H. Reneker, Sol. Energy Mater. Sol. Cells 85 (2005) 477.
[13] C. Klingshirn, Chem. Phys. Chem. 8 (2007) 782.
[14] N. Izyumskaya, V. Avrutin, U. Ozgur, Y.I. Alivov, H. Morkoc, Phys. Status Solidi B 244 (2007) 1439.
[15] D. Li, Y. Xia, Nano Lett. 3 (2003) 555.
[16] E.T. Bender, R. Wang, M.T. Aljarrah, E.A. Evans, R.D. Ramsier, J. Vac. Sci. Technol. A 25 (2007) 922.
[17] D. Li, J.T. McCann, M. Gratt, Y. Xia, Chem. Phys. Lett. 394 (2004) 387.
[18] R. Chandrasekar, L. Zhang, J.Y. Howe, N.E. Hedin, Y. Zhang, H. Fong, J. Mater. Sci. 44 (2009) 1198.
[19] C. Tekmen, A. Suslu, U. Cocen, Mater. Lett. 62 (2008) 4470.
[20] J. Zhao, C. Jia, H. Duan, H. Li, E. Xie, J. Alloys Compd. 461 (2008) 447.
[21] E.T. Bender, P. Katta, G.G. Chase, R.D. Ramsier, Surf. Interface Anal. 38 (2006) 1252.
[22] J.-A. Park, J. Moon, S.-J. Lee, S.-C. Lim, T. Zyung, Curr. Appl. Phys. 9 (2009) S210.
[23] Z. Zhu, L. Zhang, J.Y. Howe, Y. Liao, J.T. Speidel, S. Smith, H. Fong, Chem. Commun. 2009 (2009) 2568.
[24] R. Siddheswaran, R. Sankar, M. Ramesh Babu, M. Rathnakumari, R. Jayavel, P. Murugakoothan, P. Sureshkumar, Cryst. Res. Technol. 41 (2006) 446.
[25] X. Yang, C. Shao, H. Guan, X. Li, J. Gong, Inorg. Chem. Commun. 7 (2004) 176.
[26] J. Yuh, L. Perez, W.M. Sigmund, J.C. Nino, Physica E 37 (2007) 254.
[27] C. Shao, X. Yang, H. Guan, Y. Liu, J. Gong, Inorg. Chem. Commun. 7 (2004) 625.
[28] J. Moon, J.-A. Park, S.-J. Lee, S.C. Lim, T. Zyung, Curr. Appl. Phys. 9 (2009) S213.
[29] P. Viswanathamurthi, N. Bhattarai, H.Y. Kim, D.R. Lee, Nanotechnology 15 (2004) 320.
[30] R.W. Tuttle, A. Chowdury, E.T. Bender, R.D. Ramsier, J.L. Rapp, M.P. Espe, Appl. Surf. Sci. 254 (2008) 4925.
[31] C. Wang, C. Shao, L. Wang, L. Zhang, X. Li, Y. Liu, J. Colloid Interface Sci. 333 (2009) 242.
[32] NIST Chemistry Database.
[33] J.A. Munoz-Lopez, J.A. Toledo, J. Escobar, E. Lopez-Salinas, Catal. Today 133–135 (2008) 113.
[34] S.U.M. Khan, M. Al-Shahryv, W.B. Ingler Jr., Science 297 (2002) 2243.
[35] B. Zhou, Y. Wu, L. Wu, K. Zou, H. Gai, Physica E 41 (2009) 705.